A General Orthogonal Transform Aided MIMO Design for Reliable Maritime Visible Light Communications

Guixun Huang, Lin Zhang *Senior Member, IEEE*, Yuan Jiang *Member, IEEE*, Zhiqiang Wu, *Senior Member, IEEE*

Abstract—In maritime visible light communication (VLC) systems, user information is delivered among different terminals distributed in the atmosphere and the underwater environment. To combat the complex and variant marine channel conditions induced by the absorption, scattering, and turbulence influence, in this paper, we propose a general orthogonal transform (OT) aided multiple input multiple output (MIMO) transmission scheme to enhance the transmission reliability performances. In our design, we propose to construct the orthogonal transform matrix recursively with the Hadamard matrix. Thus we could exploit the repetitive property of the elements in the orthogonal matrix to enlarge the Euclidean distances among the signals. Moreover, the value of the elements could be adjusted dynamically to adapt to time-changing channel conditions. Thanks to the orthogonality of the matrix and the singular value decomposition (SVD), the interferences among signals could be effectively suppressed. Accordingly, the reliability performances can be improved. Furthermore, we derive the theoretical symbol error rate (SER) expressions for the proposed design. Numerical simulations are performed to validate the theoretical analysis. Furthermore, the SER performances with different water types and wind speeds in various scenarios of the atmosphere, underwater, and air-water interface channels are investigated and compared with the counterpart systems.

Index Terms—Air and underwater channels; maritime visible light communication; multiple input multiple output; orthogonal transform; reliability.

I. Introduction

VISIBLE light communication (VLC) has attracted great research interests in recent years thanks to certain ad-
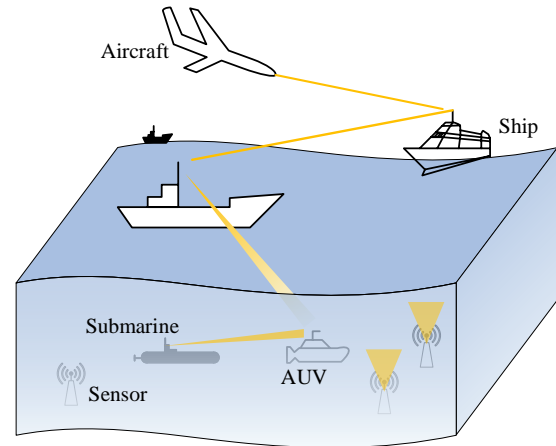
Fig. 1. Maritime VLC transmissions in the atmosphere and underwater scenarios.

vantages over traditional wireless transmission methods. On the one hand, the free-space optical (FSO) communication enjoys unlicensed spectrum resources and low electromagnetic interferences compared to radio frequency (RF) communication in terrestrial environments [1]. On the other hand, in the underwater transmission scenario, underwater wireless visible light communication (UWVLC) undergoes less attenuation than RF channels, and provides a higher data rate than that of the traditional underwater acoustic communication [2].

In practical maritime communication systems, as presented in Fig. 1, the user information might be transferred from aircraft to ships via the air-to-air link, ships to submarines via the air-to-water link, or among undersea sensors, submarines, and autonomous underwater vehicles (AUV) via the underwater link. As mentioned in [2], over optical channels, the underwater link distance would be about a hundred meters. As to the air-to-air link, the distance could be several kilometers when there exists turbulence [3]. In addition, for implementations of air-water optical communications, movable ships or unmanned aerial vehicles (UAVs) could provide more flexible and inexpensive transmission services than buoys as the surface nodes [4]. References [5] and [6] have presented optical communication systems which integrate the underwater platforms with the terrestrial or space platform, and investigated the underwater channel transmission performances as well as the experiment implementations.

In the considered VLC system model given in Fig. 1, for

both atmosphere and underwater scenarios, VLC suffers from the attenuation loss and turbulence scintillation effects during the propagations. Besides, when light travels through the water surface, the rough air-water interface might induce severe signal distortions.

To mitigate the turbulence effect, multiple input multiple output (MIMO) technique has been applied in the VLC system to enhance the system reliability by exploiting the spatial diversity. For underwater transmissions, [7] and [8] applied the single input multiple output (SIMO) and multiple input single output (MISO) scheme, respectively, to combat the underwater turbulence. Moreover, [9], [10] modeled the turbulence effect with the log-normal distribution and analyzed the optical system performances with different MIMO configurations under the weak turbulence. For transmissions over atmospheric channels, [11] used the log-normal and gamma-gamma distribution to describe the weak and strong atmospheric turbulence conditions and analyzed the bit error rate (BER) performance as well as the channel capacity when using binary phase-shift keying subcarrier-intensity modulation (BPSK-SIM). Besides, [12] studied the turbulence influence on the FSO system with different turbulence models and [13]–[15] proposed to apply MIMO techniques in FSO systems to mitigate the channel turbulence, wherein [13] derived the exact bit error rate (BER) expression for the spatial correlated MIMO system. Moreover, [15] proposed to take into account the pointing errors induced by the building sway in the channel response estimations. Except for these research achievements, which improve the reliability performances by exploiting the repetitive transmission principle or the space diversity gain, [16] and [17] have respectively proposed to utilize the spatial multiplexing (SMP) and spatial modulation (SM) schemes to improve the MIMO performance. Moreover, although [16] and [17] did not investigate the reliability performances of VLC systems in the maritime scenario, the proposed design could be generally applied in indoor or outdoor VLC systems. Furthermore, comprehensive performance comparisons of the repetitive coding (RC), SM and SMP aided MIMO schemes have also been provided.

However, little research has been done to investigate the transmission performance when the light penetrates the air-water interface. Besides, most of the schemes proposed for the reliability enhancement of MIMO systems utilize the repetitiveness in the spatial domain, few research works have been done on exploiting the repetitiveness in the time domain or the code domain.

Different from these existing research works on VLC systems, in this paper, we utilize the repetitiveness in both the time domain and the spatial domain to enhance the reliability performances. Moreover, we study the VLC system operating in practical maritime scenarios involving the transmission over the atmosphere channel, the underwater channel and the air-water interfacing channel. To be more explicit, to enhance the capability to combat the variant channel conditions, we propose an orthogonal transform (OT) aided MIMO transmission scheme to improve the system reliability performances. Notably, the proposed design can be generally applied to MIMO systems with different MIMO orders and the parameters of the orthogonal transform can be adjusted flexibly according to the channel conditions. Moreover, we also provide the comprehensive comparison with the systems applying RC, SMP, and SM schemes when there exist turbulence in channels.

In our design, the bitstream generated from users is first mapped onto the pulse amplitude modulation (PAM) symbols. After that, the PAM symbol streams are modulated by the orthogonal transform module to implement the orthogonal transformation, which is combined with the singular value decomposition (SVD) based precoder to eliminate the interferences among multiple users. At the receiver, after removing the user interference, the output signal of each transmit aperture is equivalent to that goes through a parallel channel, and the joint detection is performed on the signal vector to recover the data. Since the proposed orthogonal transform design helps to enlarge the minimum Euclidean distances among signals, the capability to combat the variant channel conditions is enhanced and the reliability performances are improved.

In addition, for the proposed OT-aided MIMO VLC system, we derive the theoretical symbol error rate (SER) expression. Subsequently, numerical simulations are performed to validate the theoretical analysis. Next, based on the atmosphere channel model in [11], the underwater channel model in [9], and the air-water interface channel model given in [18], we analyze the performances of the proposed system and compare them with those of the counterpart schemes to validate the theoretical derivations, and demonstrate that more reliable services can be achieved by our design.

Briefly, the main contributions of this paper include:

1) We propose to utilize the repetitiveness in both the spatial domain and the time domain to enhance the reliability performances. Then we propose a general OT-aided MIMO scheme to combat the complicated and variant channel conditions of maritime channels, with the aim to enhance the system reliability performance.
2) We propose to construct the multi dimension orthogonal matrix based on the Hadamard matrix recursively in order that the proposed design can be generally applied to MIMO systems with any MIMO orders. Meanwhile, the parameters in the constructed orthogonal transform matrix can be adjusted according to the channel conditions, thus the flexibility can be greatly enhanced.
3) We analyze the theoretical SER performance for the proposed system using the maximum likelihood (ML) detection at the receiver to provide an insight into the transmission behavior of the proposed system. Then we provide simulation results over maritime VLC channels, including the atmosphere channel, the underwater channel and the air-water interface channel to validate the proposed design.

The rest of the paper is organized as follows. Section II presents the details of the maritime VLC channel characteristics. In Section III, we propose the orthogonal transform aided MIMO VLC multiuser system design and provide the performance analysis. Subsequently, Section IV shows the simulation results, finally Section V concludes this paper.

II. MARITIME VLC CHANNEL MODEL

Here we describe the maritime VLC channel model in detail, including the atmosphere/underwater channel and the atmosphere-water interface channel. In the considered model, without loss of generality, we assume that perfect alignment could be achieved by the tracking, pointing and acquisition mechanisms [19] [20], thus the misalignment effects induced by the mobility of terminals on the channel conditions are negligible.

1) Atmosphere/underwater channel: Based on the light propagation characteristics, the maritime VLC channel coefficient h in both atmosphere and underwater regimes can be modeled as the combination of the path attenuation and the turbulence-induced fading [9], [11], i.e.

$$h = h_l \cdot h_t \tag{1}$$

where h_l is the path loss coefficient which indicates the light absorption and scattering characteristic along the propagation path, h_t is the channel fading induced by the turbulence.

In the atmosphere scenario, the path loss is mainly induced by molecular absorption and aerosol scattering suspended in the air, h_l is calculated by the widely used Lambert's law [21] given in (2),

$$h_l = \frac{A}{\pi(\phi L/2)^2} \exp(-\beta_v L) \tag{2}$$

where A is the receiver's aperture area, L is the propagation distance, ϕ is the divergence angle in radian and β_v is the atmosphere extinction coefficient. In the underwater scenario, we apply the Monte Carlo (MC) method [22] to calculate h_l since particles or other components in the water are dependent on water types and have great impacts on the light absorption and scattering, which can hardly be modeled with an explicit expression.

The channel response h_t is related to the turbulence effects existent in both underwater and atmosphere scenarios, which is induced by the refractive index variation in the propagation path. The turbulence would lead to the light intensity fluctuations characterized by the log-irradiance variance $\sigma_{\ln I}^2$ [9], [23], which is expressed as

$$\sigma_{\ln I}^2 = 8\pi^2 k^2 \int_0^L \int_0^\infty \kappa \Phi_n(\kappa)$$
$$\times \left[1 - \cos\left(\frac{\kappa^2 z}{k}(1 - (1-\Theta)z)\right)\right] d\kappa dz \tag{3}$$

where $\Theta = 0$ and 1 represent the spherical waves and plane waves, respectively, k is the wave number, κ and $\Phi_n(\kappa)$ denote the scalar spatial frequency and the power spectrum of turbulent fluctuations, respectively, I is the received signal intensity.

To elaborate a bit further, the log-irradiance variance for the underwater or the atmosphere channel can be calculated by substituting the corresponding power spectrum function $\Phi_n(\kappa)$ into (3) [9], [23]. Moreover, for the atmosphere VLC channel, if we neglect the inner and outer-scale effects on the scintillation, the log-irradiance variance $\sigma_{\ln I}^2$ under the plane

wave condition can be simplified as the Rytov variance σ_R^2 given by [21], [23]

$$\sigma_{\ln I}^2 = \sigma_R^2 = 1.23 C_n^2 k^{7/6} L^{11/6} \tag{4}$$

where C_n^2 is the index of the refractive structure parameter that determines the turbulence strength, with the value varying from 10^{-17} to 10^{-12}. Notably, the scintillation index (SI) σ_I^2 can be evaluated by $\sigma_I^2 = \frac{\mathbb{E}[I^2] - \mathbb{E}^2[I]}{\mathbb{E}^2[I]}$. Based on the weak fluctuation theory, we have $\sigma_I^2 = \exp(\sigma_{\ln I}^2) - 1 \cong \sigma_{\ln I}^2$ [23].

In the case of weak turbulence, i.e. $\sigma_I^2 < 1$, h_t can be modeled as the log-normal distribution [9], [13] given by

$$f(h_t) = \frac{1}{\sqrt{2\pi}\sigma_{\ln I} h_t} \exp\left(-\frac{(\ln(h_t) + \sigma_{\ln I}^2/2)^2}{2\sigma_{\ln I}^2}\right). \tag{5}$$

In moderate or strong turbulence regimes, h_t is modeled as the gamma-gamma distribution, whose probability density function is given by [11], [24],

$$f(h_t) = \frac{2(\alpha\beta)^{(\alpha+\beta)/2}}{\Gamma(\alpha)\Gamma(\beta)} h_t^{(\alpha+\beta)/2-1} K_{\alpha-\beta}(2\sqrt{\alpha\beta h_t}) \tag{6}$$

where $\Gamma(\cdot)$ denotes the gamma function, $K_{\alpha-\beta}(\cdot)$ represents the modified Bessel function of the second kind and order $\alpha - \beta$. The values of α and β are calculated by

$$\alpha = \left\{\exp\left[\frac{0.49\sigma_R^2}{(1 + 1.11\sigma_R^{12/5})^{7/6}}\right] - 1\right\}^{-1} \tag{7}$$

$$\beta = \left\{\exp\left[\frac{0.51\sigma_R^2}{(1 + 1.69\sigma_R^{12/5})^{5/6}}\right] - 1\right\}^{-1} \tag{8}$$

It is noticeable that for underwater VLC channels, σ_R^2 would be replaced by $\sigma_{\ln I}^2$.

2) Air-water interface channel: The air-water interface channel is more complicated than the atmosphere or the underwater VLC channel, as the light beam may suffer distortion when it transverses through the rough sea surface.
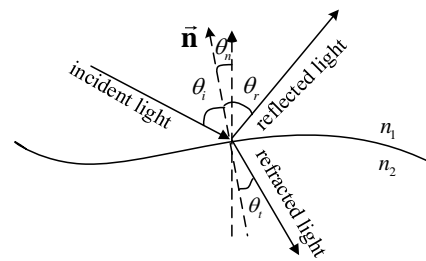
Fig. 2. Light propagation in the sea surface

As shown in Fig. 2, when a light beam reaches the water surface, part of the light energy is reflected while the rest is refracted by the surface and continues to propagate.

Here we apply the Monte Carlo method to simulate the air-water interface channel response in the regime of the wavy surface [18]. In the construction of the air-water interface channel, the procedure of the photon propagation in the atmosphere or underwater channel is modelled as that the photons move in a homogeneous medium without the variation

of the refractive index [22], [25], while the refractive index changes from n_1 to n_2 at the air-water interface.

In this case, the photon would reflect on the interface or refract into the water. The probability of the event that a photon takes the refraction is determined by the reflectance $\mathcal{R}$ denoted as [18]

$$\mathcal{R} = \frac{1}{2} \left[\frac{\sin^2(\theta_i - \theta_t)}{\sin^2(\theta_i + \theta_t)} + \frac{\tan^2(\theta_i - \theta_t)}{\tan^2(\theta_i + \theta_t)} \right] \quad (9)$$

where θ_i is the incidence angle of photon, θ_t is the refraction angle that can be calculated through the Snell's law represented by $\frac{n_1}{n_2} = \frac{\sin \theta_t}{\sin \theta_i}$.

Note that the incidence angle θ_i and refraction angle θ_t are determined with respect to the normal vector $\vec{n}$ of the water surface. When the sea surface fluctuates with the wind, the direction of $\vec{n}$, which is represented by its azimuth angle θ_z and polar angle θ_n, varies accordingly. It is worth mentioning that θ_z is uniformly distributed in $[0, 2\pi]$, while the distribution of θ_n is given by [18]

$$p(\theta_n) = \frac{2}{\sigma^2} \exp \left(\frac{-\tan^2 \theta_n}{\sigma^2} \right) \tan \theta_n \sec^2 \theta_n \quad (10)$$

where σ^2 is the mean square slope of the sea surface related to the wind speed V given by $\sigma^2 = 0.003 + 0.00512V$. Thus, under certain wind speed, the direction of $\vec{n}$ can be generated randomly according to the distribution given in (10).

Take the mixed interface channel which includes a 100-meter atmosphere link and a 20-meter clear water link as an example. At each loop of our MC simulations, a number of photons start from an initial point which is located 100 meters above the sea and reach the air-water interface in various incidence angles. Then in the surface plane, a fraction of photons will refract into the underwater region to reach the receiving plane, while the rest will reflect. By counting the photon statistics in the receiver along with the arrival time of the photons, the received light intensity and the channel impulse response (CIR) can be attained.
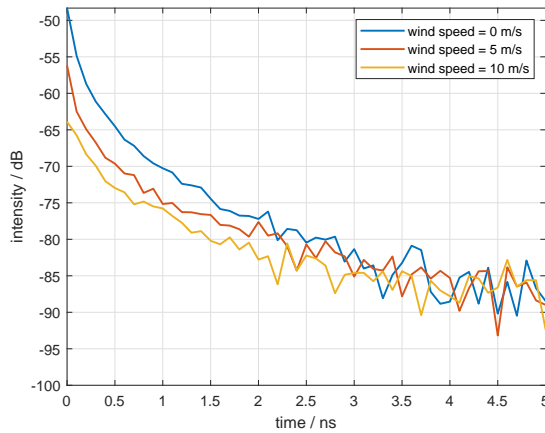

Fig. 3. CIR of the interface channel under different wind speeds

Figure 3 shows the CIR results under different wind speed conditions, in which the number of the simulated photons is set as 10^7, the receiver aperture diameter is 0.05 m and the field

of view (FOV) of the aperture is $90°$. Based on the definition of the time dispersion τ [22], which equals to the duration that CIR falls 20 dB below its peak, from Fig. 3, we can observe that the largest time dispersion τ is about 3 ns on the condition that the wind speed is 10 m/s. Therefore, when the data rate is not higher than the level of Gbps, the channel time dispersion can be neglected. In the follow system design and performance analysis, we treat the maritime VLC channel as non-dispersive.

III. OT-AIDED MIMO VLC SYSTEM

This section, we will present the MIMO-based VLC multiuser transmitter as well as the receiver structures and propose the orthogonal transform design. Then theoretical performance analysis is provided.
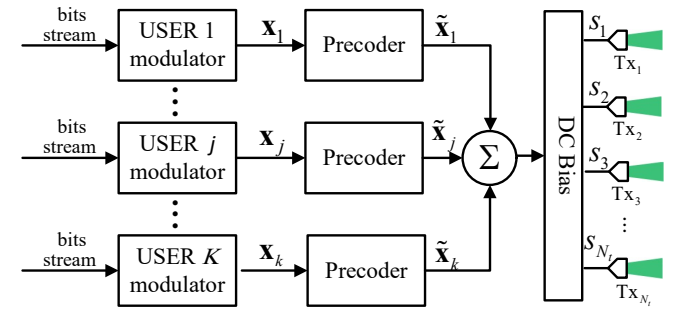
A. MIMO Multiuser Transmitter

Fig. 4. Transmitter structure for multiuser VLC system.

In a MIMO-based VLC system, a base station, which might be a ship in the ocean, would simultaneously transmit data to multiple users such as AUVs or submarines. As illustrated in Fig. 4, N_t transmit apertures in the base station deliver data to K users, while the jth user receives data with $N_{r,j}$ apertures (receivers). Hence, the number of all user receivers is given as $N_r = \sum_{j=1}^{j=K} N_{r,j}$.

In the transmitter structure, the user data is first modulated by the proposed orthogonal transform aided modulator to be elaborated in the following subsection III-B. Let $\mathbf{x}_j$ denote the modulated signal that is to be transferred to the user j. After the precoding operation performed on $\mathbf{x}_j$, the resultant $N_t \times 1$ signal $\tilde{\mathbf{x}}_j$ is expressed as

$$\tilde{\mathbf{x}}_j = \mathbf{P}_j \mathbf{x}_j \quad (11)$$

where $\mathbf{P}_j$ is the precoding matrix for user j.

To elaborate a bit further, $\mathbf{P}_j$ is constructed through the SVD operation [17] in the precoder module to suppress the multi-user interferences (MUIs). Without loss of generality, we assume that both the transmitter and the receiver know the prefect channel state information (CSI), which can be obtained from the feedback of the receiver or through the channel estimation at the transmitter [17]. Define the $(N_r - N_{r,j}) \times N_t$ complementary channel matrix $\tilde{\mathbf{H}}_j$ for the jth user as $\tilde{\mathbf{H}}_j = [\mathbf{H}_1^T \cdots, \mathbf{H}_{j-1}^T, \mathbf{H}_{j+1}^T \cdots, \mathbf{H}_K^T]^T$, and the rank of it is $\tilde{L}_j$,

then in the jth precoder, performing the SVD operation on $\tilde{\mathbf{H}}_j$ and the jth user's equivalent channel matrix $\bar{\mathbf{H}}_j$, we have:

$$\tilde{\mathbf{H}}_j = \tilde{\mathbf{U}}_j \tilde{\mathbf{\Lambda}}_j \left[\tilde{\mathbf{V}}_j^{(1)} \mid \tilde{\mathbf{V}}_j^{(0)} \right]^T \tag{12}$$

$$\bar{\mathbf{H}}_j = \mathbf{H}_j \tilde{\mathbf{V}}_j^{(0)} = \mathbf{U}_j \mathbf{\Lambda}_j \mathbf{V}_j^T \tag{13}$$

where $\bar{\mathbf{H}}_j$ is a $N_{r,j} \times (N_t - \tilde{L}_j)$ matrix, the orthogonal matrices $\tilde{\mathbf{U}}_j$, $\mathbf{U}_j$, $\mathbf{V}_j$ are of the size of $(N_r - N_{r,j}) \times (N_r - N_{r,j})$, $N_{r,j} \times N_{r,j}$ and $(N_t - \tilde{L}_j) \times (N_t - \tilde{L}_j)$, respectively. $\mathbf{H}_j$ is the channel matrix corresponds to user j, whose size is $N_{r,j} \times N_t$. The $N_t - \tilde{L}_j$ columns in matrix $\tilde{\mathbf{V}}_j^{(0)}$ are the basis vectors that form the null space of $\tilde{\mathbf{H}}_j$, which follows that $\tilde{\mathbf{H}}_j \cdot \tilde{\mathbf{V}}_j^{(0)} = \mathbf{0}$. The $(N_r - N_{r,j}) \times N_t$ matrix $\tilde{\mathbf{\Lambda}}_j$ and $N_{r,j} \times (N_t - \tilde{L}_j)$ matrix $\mathbf{\Lambda}_j$ are two diagonal matrices whose elements are the singular values of $\tilde{\mathbf{H}}_j$ and $\bar{\mathbf{H}}_j$, respectively.

Thus, by using (12) and (13), based on the concept of the null space, the $N_t \times (N_t - \tilde{L}_j)$ precoding matrix $\mathbf{P}_j$ is obtained as

$$\mathbf{P}_j = \tilde{\mathbf{V}}_j^{(0)} \mathbf{V}_j \tag{14}$$

When N_t is equal to N_r and matrix $\tilde{\mathbf{H}}_j$ is of full rank, we have $N_t - \tilde{L}_j = N_{r,j}$ and the size of $\mathbf{x}_j$ is $N_{r,j} \times 1$. Then we could obtain the transmitted vector $\mathbf{s}$ as:

$$\mathbf{s} = \sum_{j=1}^{K} (\tilde{\mathbf{x}}_j) + \mathbf{d} = \sum_{j=1}^{K} (\mathbf{P}_j \mathbf{x}_j) + \mathbf{d} \tag{15}$$

where the direct current (DC) bias $\mathbf{d}$ is added in the end to guarantee the transmitted signal to be non-negative. Finally, these signals $\mathbf{s} = [s_1, s_2 \ldots s_{N_t}]^T$ are transmitted via N_t transmit aperture over channels.

B. Orthogonal Transform Scheme

In this subsection, we neglect the subscript of the parameters for any specific user for the sake of brevity, e.g. we use $\mathbf{x}$ to represent $\mathbf{x}_j$ for the jth user.
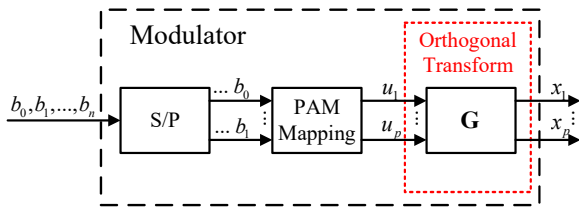

Fig. 5. Block diagram of the orthogonal transform aided modulator.

1) Orthogonal transform aided modulator: As mentioned above, the user data are first modulated by the modulator before precoding. Figure 5 presents the block diagram of the orthogonal transform aided modulator structure. Specifically, after the serial to parallel (S/P) conversion, the bitstream is modulated into PAM symbols, i.e. $u_1, u_2, \ldots, u_p \in \mathbb{U}$, where $\mathbb{U}$ denotes the M-PAM constellation, the value of p corresponds to the quantity of $N_t - \tilde{L}_j$. Subsequently, the PAM vector $\mathbf{u} = [u_1, u_2, \ldots, u_p]^T$ is transformed by the orthogonal matrix $\mathbf{G}$ with the dimension of $p \times p$ shown as below:

$$\mathbf{x} = \mathbf{G} \cdot \mathbf{u} \tag{16}$$

where $\mathbf{x}$ is the output vector that will be delivered to the precoder. Notably, with the aid of the orthogonal transform performed on the PAM vector, the power of each PAM symbol in the original vector is equivalently reallocated, and since matrix $\mathbf{G}$ is orthogonal, the average power of the transformed vector $\mathbf{x}$ remains the same as $\mathbf{u}$.

2) Determination of orthogonal matrix $\mathbf{G}$: In our system, the Euclidean distances under the fading channel [26] between any two transmitted vectors is given by,

$$d = \|\mathbf{\Lambda}(\mathbf{x}^i - \mathbf{x}^j)\|_F^2 = \|\mathbf{\Lambda}\mathbf{G}(\mathbf{u}^i - \mathbf{u}^j)\|_F^2 \tag{17}$$

where $\mathbf{\Lambda}$ is the singular matrix derived from (13), $\mathbf{x}^i$ and $\mathbf{x}^j, i \neq j$ are two different transformed vectors, $\|\cdot\|_F$ denotes the Frobenius norm, and $\mathbf{u}^i, \mathbf{u}^j \in \mathbb{U}^{p \times 1}$ are the corresponding modulated PAM vectors. Since the detection error event of a specific vector under ML criterion is mainly determined by its minimum distance to the other vectors [27], from (17), the minimum distance of a vector $\mathbf{x}^i$ to other vectors in the receiver is given as (18),

$$d_{\min}^i = \min_{j=1,\ldots,M^p, j \neq i} \|\mathbf{\Lambda}\mathbf{G}(\mathbf{u}^i - \mathbf{u}^j)\|_F^2 \tag{18}$$

which indicates that the choice of matrix $\mathbf{G}$ would influence the system reliability performances.

To be more explicit, define $\Delta\mathbb{U}$ as the set of the PAM vector differences, whose element $\Delta\mathbf{u}^{ij} = \mathbf{u}^i - \mathbf{u}^j, i \neq j$ is the difference of vector $\mathbf{u}^i$ and $\mathbf{u}^j$. From (18), the system reliability can be enhanced by selecting a proper orthogonal matrix $\mathbf{G}$ such that the minimum distance among all the received vectors is maximized, i.e.

$$\begin{aligned} \text{find}: \quad & \mathbf{G} \\ \text{maximize}: \quad & \min_{\Delta\mathbf{u}^{ij} \in \Delta\mathbb{U}} \|\mathbf{\Lambda}\mathbf{G}\Delta\mathbf{u}^{ij}\|_F^2 \end{aligned} \tag{19}$$

Furthermore, the expression in (19) can be further expanded as,

$$\begin{aligned} \|\mathbf{\Lambda}\mathbf{G}\Delta\mathbf{u}^{ij}\|_F^2 &= (\mathbf{G}\Delta\mathbf{u}^{ij})^T \mathbf{\Lambda}^2 (\mathbf{G}\Delta\mathbf{u}^{ij}) \\ &= \mathbf{z}^T \mathbf{\Lambda}^2 \mathbf{z} \\ &= \sum_{k=1}^{p} \lambda_k^2 \cdot z_k^2 \end{aligned} \tag{20}$$

where $\mathbf{z}$ is the transformed version of $\mathbf{G}\Delta\mathbf{u}^{ij}$, z_k is the kth element of $\mathbf{z}$ and λ_k is the kth diagonal element of $\mathbf{\Lambda}$. To elaborate a bit further, (19) achieves the maximization of the minimum length of the vectors, which are obtained from the transformation of $\Delta\mathbf{u}^{ij}$ with $\mathbf{G}$ and the scaling with $\mathbf{\Lambda}$.

For example, when $p = 2$, the orthogonal matrix can have the form of

$$\mathbf{G}_{2\times 2}(a, b) = \begin{bmatrix} b & -a \\ a & b \end{bmatrix} \tag{21}$$

where a and b are elements of the matrix which should be respectively real number in our VLC systems. In practical underwater VLC system, it is expected that the transmitting power remains constant. To meet this demand, a and b should be normalized by $\sqrt{a^2 + b^2} = 1$. Thus both a and b should have the value in the range of $[-1, 1]$.

As the vectors $\Delta\mathbf{u}^{ij} \in \Delta\mathbb{U}$ are discrete, the problem in (19) is not a linear problem, hence we apply the traversal

---

Algorithm 1 Search algorithm for a

Input: channel singular value matrix $\mathbf{\Lambda}$
Output: a
1: initialize $g_0 = 0, a_0 = -1$
2: **for** $\dot{a} = [-1, 1]$ **do**
3:     $d_0 = \inf$
4:     **for** $i = 1 : M^p - 1$ **do**
5:        $t_0 = \inf$
6:        **for** $j = i + 1 : M^p$ **do**
7:           calculate $\dot{b} = \sqrt{1 - \dot{a}^2}$;
8:           calculate $\mathbf{G}_{p \times p} = \frac{1}{\sqrt{2}} \cdot \mathbf{D}_{2^k} \otimes \mathbf{G}_{2\times2}(\dot{a}, \dot{b})$;
9:           calculate $t_1 = \|\mathbf{\Lambda}\mathbf{G}_{p \times p}\Delta\mathbf{u}_{ij}\|_F^2$;
10:          **if** $t_1 \leq t_0$ **then**
11:             $t_0 = t_1$;
12:          **end if**
13:        **end for**
14:        **if** $t_0 \leq d_0$ **then**
15:           $d_0 = t_0$;
16:        **end if**
17:     **end for**
18:     **if** $d_0 \geq g_0$ **then**
19:        $a_0 = \dot{a}, g_0 = d_0$;
20:     **end if**
21: **end for**
22: Return $a = a_0$.

---

searching method to find the optimal value of a or b. Moreover, considering that a and b can be derived each other from $\sqrt{a^2 + b^2} = 1$, naturally we here only discuss how to calculate a as presented by Algorithm 1.

When the MIMO order is higher, the dimension of $\mathbf{G}$, i.e. $p \times p$ will also has a larger value. According to the expression of the Hadamard matrix $\mathbf{D}_{2^k}$ with the dimension of $2^k \times 2^k$ given by

$$\mathbf{D}_{2^k} = \frac{1}{\sqrt{2}}\begin{bmatrix} \mathbf{D}_{2^{k-1}} & \mathbf{D}_{2^{k-1}} \\ \mathbf{D}_{2^{k-1}} & -\mathbf{D}_{2^{k-1}} \end{bmatrix} \tag{22}$$

where $\mathbf{D}_1 = 1$, we could derive the expression of the orthogonal matrix $\mathbf{G}$ as

$$\mathbf{G}_{p \times p} = \frac{1}{\sqrt{2}} \cdot \mathbf{D}_{2^k} \otimes \mathbf{G}_{2\times2}(a, b) \tag{23}$$

where $p = 2^{k+1}$, $\otimes$ denotes the Kronecker product. Then based on the searching steps in Algorithm 1 we could find the optimal value of a and attain the orthogonal matrix $\mathbf{G}$. Note that in the VLC transmission, the orthogonal matrix $\mathbf{G}$ is updated along with the CSI in each transmission time slot. Namely, the matrix $\mathbf{G}$ used for the transmitter can be updated either from the feedback of the receiver or the CSI shared between transceivers.

C. Receiver Structure

The receiver structure for the jth user is shown in Fig. 6, in which the received signal vector $\mathbf{y}_j$ can be expressed by

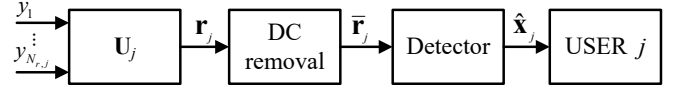$$\mathbf{y}_j = \mathbf{H}_j\mathbf{s} + \mathbf{n}_j \tag{24}$$

Fig. 6. Receiver structure for the jth user.

where $\mathbf{n}_j$ with the dimension of $N_{r,j} \times 1$ is the additive white Gaussian noise (AWGN) vector, which is of zero mean with the variance as $\sigma_n^2 = \sigma_{bg}^2 + \sigma_{dc}^2 + \sigma_{th}^2$, where $\sigma_{bg}^2, \sigma_{dc}^2, \sigma_{th}^2$ denote the variance of background noise, dark current noise and thermal noise, respectively [7]. $\mathbf{H}_j$ is the channel matrix for user j and has the dimension of $N_{r,j} \times N_t$, its element h_{mn} is the channel gain of the nth transmit aperture and mth aperture of user j.

Using the matrix $\mathbf{U}_j$ derived in (13), the received signals are transformed by $\mathbf{r}_j = \mathbf{U}_j^T\mathbf{y}_j$. Since $\mathbf{H}_j \cdot \tilde{\mathbf{V}}_i^{(0)} = \mathbf{0}, i \neq j$, after the removal of the DC component, we have

$$\bar{\mathbf{r}}_j = \mathbf{\Lambda}_j\mathbf{x}_j + \mathbf{U}_j^T\mathbf{n}_j = \mathbf{\Lambda}_j\mathbf{G}_j\mathbf{u}_j + \mathbf{U}_j^T\mathbf{n}_j \tag{25}$$

where $\mathbf{G}$ is the orthogonal matrix for the user j. For the diagonal matrix $\mathbf{\Lambda}_j$, $\bar{\mathbf{r}}_j$ can be reexpressed as

$$\bar{\mathbf{r}}_j = \begin{bmatrix} \bar{r}_1 \\ \vdots \\ \bar{r}_{N_{r,j}} \end{bmatrix} = \begin{bmatrix} \lambda_1 x_1 \\ \vdots \\ \lambda_{N_{r,j}} x_{N_{r,j}} \end{bmatrix} + \begin{bmatrix} \tilde{n}_1 \\ \vdots \\ \tilde{n}_{N_{r,j}} \end{bmatrix} \tag{26}$$

where $\tilde{n}_i$ is the ith element in $\mathbf{U}_j^T\mathbf{n}_j$. Thus thanks to the orthogonality achieved by SVD, MUIs can be suppressed and the user data is equivalent to be transmitted in parallel.

Subsequently, the ML detection is carried out to recover the signal $\mathbf{x}_j$ from $\bar{\mathbf{r}}_j$, the ML detection is shown as below:

$$\hat{\mathbf{x}}_j = \arg\max_{\mathbf{x}_j} p(\bar{\mathbf{r}}_j|\mathbf{x}_j, \mathbf{\Lambda}_j) = \arg\min_{\mathbf{x}_j} \|\bar{\mathbf{r}}_j - \mathbf{\Lambda}_j\mathbf{x}_j\|_F^2 \tag{27}$$

where $\hat{\mathbf{x}}_j$ is the estimates of $\mathbf{x}_j$, and $\hat{\mathbf{x}}_j$ is delivered to user j.

Since the ML detection is implemented by finding the minimum Euclidean distance between the detected signal and the original signal, the proposed orthogonal transform aided design can effectively enlarge distances between transmitted signals with the aim to enhance the reliability performances.

D. Computational Complexity Analysis

Next, we analyze the computational complexity of the proposed transceiver. At the transmitter, the complexity is mainly determined by the traversal searching for the optimal value of a presented in Algorithm 1, while at the receiver, the complexity is dependent on the ML detection.

To be more specific, from Algorithm 1, we can see that the complexity is mainly dependent on step 8 and step 9 in the inner loop. Since in step 8, $\mathbf{D}_{2^k}$ contains $2^k \times 2^k$ elements, i.e. $(\frac{p}{2})^2$ elements, thus it requires $4 \times (\frac{p}{2})^2 = p^2$ multiplications and 0 additions. For step 9, $(p^3 + p^2 + p)$ multiplications and $(p-1)(p^2 + p + 1)$ additions are required to calculate $\mathbf{\Lambda}\mathbf{G}_{p \times p}\mathbf{u}_{ij}$ and the Frobenius norm. In total, with the assumption that the iteration times for first loop is K, since for each iteration it requires $\frac{M^{2p}}{2}$ loops, therefore, the total computational complexity is at the level of $O(M^{2p})$.

On the other hand, at the receiver, the ML detection will also perform the traversal searching to find out the symbol estimates from the received M^p symbols. Accordingly, the computational complexity will be at the level of $O(M^p)$.

Last but not the least, it is worth mentioning that although the computational complexity is relatively high due to the traversal searching, we could select the dimension of $\mathbf{G}$ or the modulation order to achieve a better tradeoff between the complexity and the reliability performances.

E. Theoretical SER Analysis

Here, we analyze the theoretical SER performance for the proposed MIMO VLC system when operating in the atmosphere or underwater scenarios wherein the channel can be characterized by a specific statistical distribution.

1) Pairwise error probability: For the ML detection based receiver, the conditional pairwise error probability (PEP) is the probability that the detector misjudges the vector $\mathbf{x}^i$ into $\mathbf{x}^j$. With the knowledge of the channel response $\mathbf{H}$ or $\mathbf{\Lambda}$, we attain the conditional PEP between $\mathbf{x}^i$ and $\mathbf{x}^j$ as:

$$
\begin{aligned}
P(\mathbf{x}^i \rightarrow \mathbf{x}^j \mid \mathbf{\Lambda}) &= Q\left(\sqrt{\frac{\Gamma \|\mathbf{\Lambda}(\mathbf{x}^i - \mathbf{x}^j)\|_F^2}{4}}\right) \\
&= Q\left(\sqrt{\frac{\Gamma \|\mathbf{\Lambda}\mathbf{G}(\mathbf{u}^i - \mathbf{u}^j)\|_F^2}{4}}\right)
\end{aligned}
\tag{28}
$$

where $\Gamma = \frac{E_s}{N_0}$ denotes the signal energy E_s to the noise power N_0 ratio.

2) Lower bound of the conditional error probability: As the detection error probability for any transmitted vector $\mathbf{x}^i$ is mainly decided by its minimum distance to the other vectors under the fading channel, from the expression of $d_{\min}^i$ given by (18), the lower bound of the conditional error probability when transmitting $\mathbf{x}^i$ is expressed as

$$
P(e \mid \mathbf{\Lambda}, \mathbf{x}^i)_{\text{BOUND}}^{\text{LOWER}} = Q\left(\sqrt{\frac{\Gamma \cdot d_{\min}^i}{4}}\right)
\tag{29}
$$

Thus the lower bound for the conditional system error probability $P(e \mid \mathbf{\Lambda})$ can be attained by averaging the conditional error probability of all the transmitted vectors [28]. Namely, according to $P(e \mid \mathbf{\Lambda}) \geq \frac{1}{M^p} \sum_{i=1}^{M^p} P(\mathbf{x}^i \rightarrow \mathbf{x}^k \mid \mathbf{\Lambda})$, where $\mathbf{x}^k$ is the vector that has the minimum distance d_{min}^i to the vector $\mathbf{x}^i$ for a specific $\mathbf{\Lambda}$, we can obtain

$$
P(e \mid \mathbf{\Lambda})_{\text{BOUND}}^{\text{LOWER}} = \frac{1}{M^p} \sum_{i=1}^{M^p} Q\left(\sqrt{\frac{\Gamma \cdot d_{\min}^i}{4}}\right)
\tag{30}
$$

3) Lower bound of the error probability: Next, we could derive the lower bound of the error probability $P_{e,l}$ by calculating the statistical average of $P(e \mid \mathbf{\Lambda})_{\text{BOUND}}^{\text{LOWER}}$ on $\mathbf{\Lambda}$ by

$$
\begin{aligned}
P_{e,l} &= \mathbb{E}_{\mathbf{\Lambda}}\left[P(e \mid \mathbf{\Lambda})_{\text{BOUND}}^{\text{LOWER}}\right] \\
&= \int_{\mathbf{\Lambda}} P(e \mid \mathbf{\Lambda})_{\text{BOUND}}^{\text{LOWER}} \cdot f(\mathbf{\Lambda}) d\mathbf{\Lambda}
\end{aligned}
\tag{31}
$$

where $f(\mathbf{\Lambda})$ represents the statistical distribution of $\mathbf{\Lambda}$, which could be derived from the distribution of $\mathbf{H}$ such as the log-normal or gamma-gamma distribution.

Furthermore, in order to reduce the complexity of evaluation of the error probability with (31), we propose to apply the MC method [29] to approximate the statistical average with the numerical average. Namely, we have

$$
P_{e,l} \approx \frac{1}{W} \sum_{w=1}^{W} P(e \mid \mathbf{\Lambda}_w)_{\text{BOUND}}^{\text{LOWER}}
\tag{32}
$$

$$
= \frac{1}{W} \sum_{w=1}^{W} \frac{1}{M^p} \sum_{i=1}^{M^p} Q\left(\sqrt{\frac{\Gamma \cdot \min_{j \neq i} \|\mathbf{\Lambda}_w \mathbf{G}(\mathbf{u}^i - \mathbf{u}^j)\|_F^2}{4}}\right)
$$

where W denotes the number of the samples, and w represents the index of the sample.

From (32), we could get the insight into the transmission behavior over the maritime channel. To be more explicit, the error probability $P_{e,l}$ obviously depends on the value of $Q(\cdot)$ function. Since $Q(\cdot)$ function is monotonically decreasing, hence larger Γ will lead to smaller error probability. Similarly, when the distance between adjacent symbols increases, i.e., for larger $\min_{j \neq i} \|\mathbf{\Lambda}_w \mathbf{G}(\mathbf{u}^i - \mathbf{u}^j)\|_F^2$, $P_{e,l}$ decreases and hence the reliability performances could be improved. In the following section, we will provide simulation results to validate the theoretical analysis.

IV. NUMERICAL RESULTS

In this section, we first validate the theoretical derivations via the comparisons with simulation results and the benchmark schemes, including the SMP scheme, SM scheme, and RC scheme [16], [17]. Then we will compare the SER performances of our proposed design with counterpart schemes under practical maritime VLC channel conditions, and provide the SER performances when different distances between transceivers, different water types and different wind speeds are considered.

TABLE I
SYSTEM PARAMETER SETTINGS

Parameters	Value
Light source	Laser
Beam width	3 mm
Beam wavelength λ_0	532 nm
Optical to electrical conversion efficiency η	1
FOV semi-angle of receiver $\Psi_{1/2}$	45°
Receiver aperture diameter D	0.05 m
Divergence semi-angle of transmitters $\Phi_{1/2}$	0.5°
Separation distance between receivers s_r	0.25 m
Separation distance between transmitters s_t	0.25 m

The system transceiver parameter settings for simulations are listed in table I. Note that in the simulated system, unless specified, the considered multiuser system is equipped with $N_t = 4$ transmit apertures, while there are $K = 2$ users and each one is amounted with $N_{r,j} = 2$ reception apertures to receive data. In this case, the size of the orthogonal matrix is 2×2, i.e., $p = 2$. In addition, the reception aperture diameter is set as 5 cm [13], hence no aperture averaging would be applied since the aperture diameter is comparable to the link coherence length. Notably, the distance between adjacent

apertures will be larger than transversal coherence length (or coherence radius) to guarantee the sub-channels established between each pair of transmitter and receiver apertures would be statistically independent from each other. Additionally, with reference to [30], the divergence semi-angle of transmitters is set as $0.5°$ to meet the coverage requirement.

For fairness of comparisons, for the same MIMO order, we set the same transmission spectral efficiency of each user, which is denoted by ζ, for our design and benchmark schemes [16] [17]. For example, when $p = 2$, if we set the transmission spectral efficiency of each user as the same 4 bit/s/Hz, then the PAM order for our proposed OT scheme and the SMP scheme is 4-PAM, while the PAM order for SM scheme is 8-PAM and RC scheme is 16-PAM. Besides, the same transmit electrical power is used in the proposed system and the counterpart schemes. Moveover, the same channel characteristic, e.g. log-normal or gamma-gamma fading distribution, would be applied for all links, with the channel characteristic of each link being independent from each other and remaining invariant during the transmission period. Additionally, the turbulence effect is considered to be coherent during each transmission period.

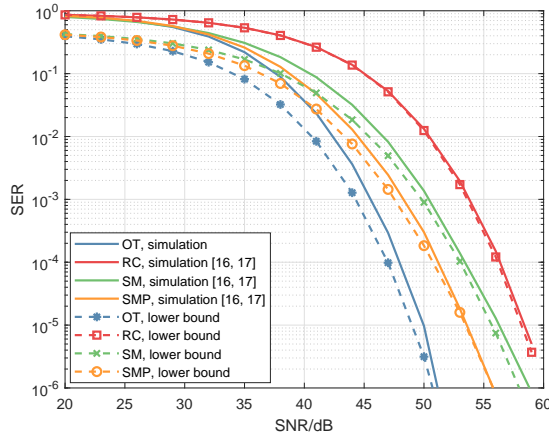## A. Theoretical and Simulated Performances

Fig. 7. Theoretical and simulated performance comparisons over the atmosphere channel, $\sigma_I^2 = 0.18$, $\zeta = 4$ bit/s/Hz, $p = 2$.

First of all, we compare the simulation results with the analytical curves. As shown in Fig. 7 and Fig. 8, the SER simulation results of different schemes fit well with the analytical lower bound in the atmosphere channel and the underwater channel, which are simulated over 500-meter atmosphere link and 20-meter clear water link, respectively. Moreover, for higher value of SNR, the lower bound of each scheme gets closer to its simulation curve, which verifies the effectiveness of our theoretical performance analysis. Besides, we can observe from the figure that the proposed OT aided system obtains better SER performances than the counterpart schemes.

B. Performance Comparisons

Figure 9 illustrates the SER performances among the proposed system and the benchmark schemes [16], [17] over the
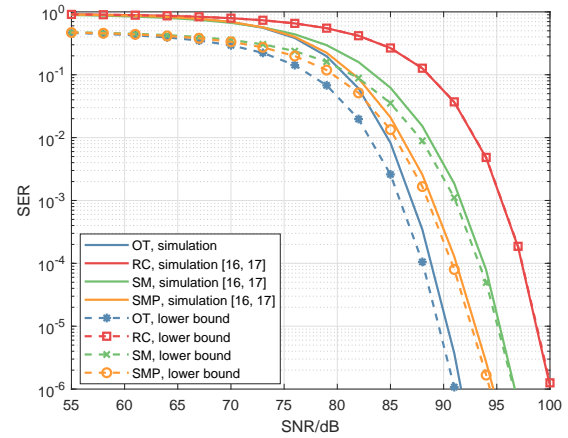

Fig. 8. Theoretical and simulated performance comparisons over the underwater channel, $\sigma_I^2 = 0.05$, $\zeta = 4$ bit/s/Hz, $p = 2$.
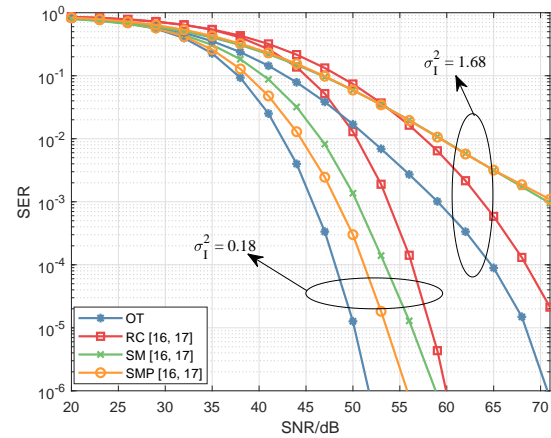

Fig. 9. Performance comparisons over the atmosphere channel, $\zeta = 4$ bit/s/Hz, $p = 2$.

atmosphere channel with the distance of 500 meters between the transceiver. In the simulations, in the weak turbulence regime with $\sigma_I^2 = 0.18$, the log-normal distribution is used to model the turbulence effect, while the gamma-gamma model with $\sigma_I^2 = 1.68$ is used for the analysis when moderate to strong turbulence exists. From the figure, it can be seen that when the turbulence becomes stronger, the SER performances become worse. Moreover, we can observe that the proposed OT aided system can combat the turbulence and achieve better reliability performances than counterpart schemes. To be more explicit, when $\sigma_I^2 = 0.18$, OT scheme outperforms the SMP scheme about 4 dB at SER = 1E-6 level, while for $\sigma_I^2 = 1.68$, the OT scheme obtains the performance gain of about 3 dB at SER = 1E-5 comparing to the RC scheme.

Figure 10 compares the SER performances when using different modulation schemes over the underwater channel. In the simulations, the transmission distance in the water is 20 meters and the water type is clear water. Both of the weak and moderate turbulence conditions are taken into account, i.e., the scintillation index of the light wave is respectively set as $\sigma_I^2 = 0.05$ and $\sigma_I^2 = 1.23$. Similar to the results attained in
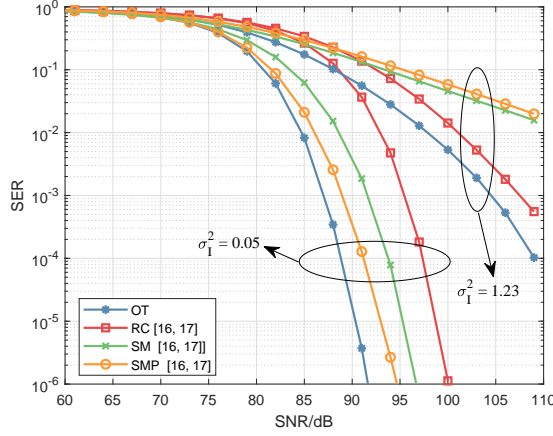
Fig. 10. Performance comparisons over the underwater channel, $\zeta = 4$ bit/s/Hz, $p = 2$.

Fig. 9, the OT aided scheme outperforms the other schemes and achieves better reliability performances when there exists the turbulence.
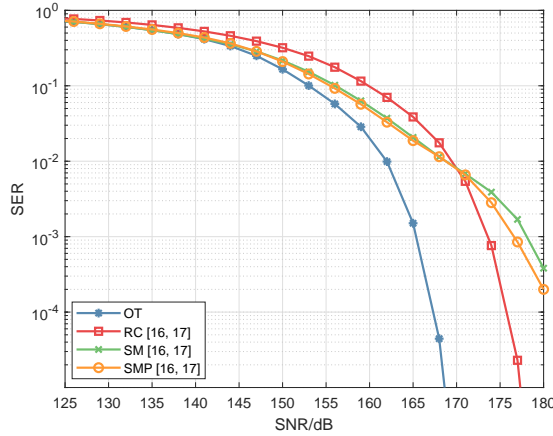

Fig. 11. Performance comparisons over the air-water interface channel, $\zeta = 4$ bit/s/Hz, $p = 2$.

Subsequently, we compare the SER performances of the proposed OT-aided system and counterpart schemes over the air-water interface channel, which consists of 100-meter atmospheric channel and 20-meter clear underwater channel, with the wind speed set as 2.5 m/s. As shown in Fig. 11, as the surface plane fluctuates continuously, the SER performances are attained by averaging the SER of 5×10^3 simulation results, while the response of each channel is attained in a random surface slope generated by MC approach presented in subsection II-2. From Fig. 11, we see that the system suffers from significant SNR losses in this scenario due to the reflection or the distortion through the interface. Furthermore, we can also observe that the OT aided scheme attains the best reliability performances compared to the other counterpart schemes.

Last but not the least, we can notice from Fig. 9, Fig. 10 and Fig. 11 that the proposed OT-aided MIMO VLC

transmission system can effectively improve the reliability performances via selecting the element value of the orthogonal matrix and enlarging the Euclidean distances. Thus better SER performances than all counterpart systems can be achieved.

C. Performances with different parameters

Next, we investigate the SER performances of the proposed OT-aided MIMO VLC system when the considered channel has different conditions.
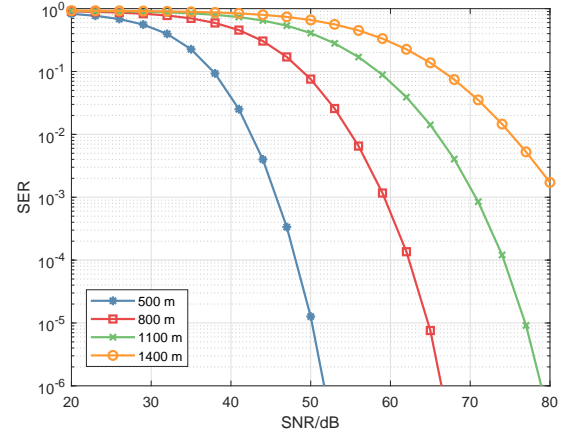

Fig. 12. SER performances over the atmosphere channel with different link distances, $\zeta = 4$ bit/s/Hz, $p = 2$.

1) Different link distances: We first study the performances of the OT-aided system over the atmosphere channel with the extinction coefficient β_υ set as 0.0005 m^{-1} and the turbulence strength of $C_n^2 = 10^{-14}$. It can be observed from Fig. 12 that when the distances between transceivers have the shortest value, the proposed system naturally achieves the best SER performances. Moreover, when the distance becomes larger, the SER performances degrade accordingly.
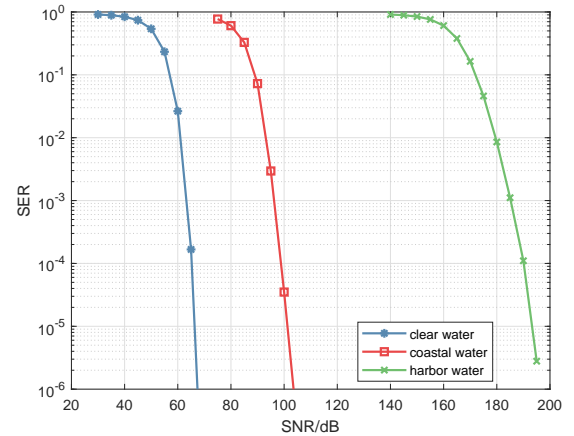

Fig. 13. SER performances over the underwater channel with different water types, $\zeta = 4$ bit/s/Hz, $p = 2$.

2) Different water types: When the proposed system operates over the underwater channel, the refraction index would be closely related to the water types, which would induce

different channel propagation conditions for the information transmission. To be more explicit, the absorption coefficient γ and extinction coefficient δ are dependent on the water types. In the clear water, the typical values of the coefficients are $\gamma = 0.069$ m^{-1} and $\delta = 0.15$ m^{-1}, while for the coastal water we have $\gamma = 0.088$ m^{-1} and $\delta = 0.305$ m^{-1}, and in the harbor water, the value becomes $\gamma = 0.295$ m^{-1} and $\delta = 2.17$ m^{-1}.

Figure 13 illustrates the SER performances of the proposed OT-aided system when the transmission distance is 10 meters, the turbulence effect is set as weak turbulence, with $\sigma_I^2 = 0.05$. It could be observed that the proposed system achieves the best SER performances in clear water, since in turbid water there are more particles or solids suspended in the transmission medium, which leads to greater absorption and scattering to the light propagation and worse SER performances. Moreover, it can be seen that the SER performances over underwater channels are worse than those over the atmosphere channel, since the signals undergo larger attenuations induced by the absorption and the scattering effects.
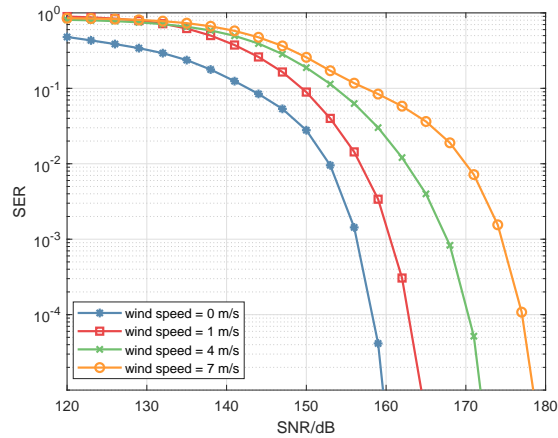
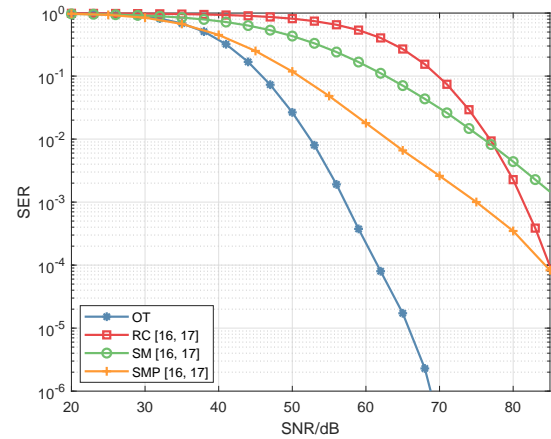the atmospheric channel with the moderate turbulence strength as the propagation channel.

Fig. 15. Performance comparisons over the atmosphere channel, $\zeta = 8$ bit/s/Hz, $p = 4$.

Fig. 14. SER performance over the air-water interface channel with different wind speeds, $\zeta = 4$ bit/s/Hz, $p = 2$.

3) Different wind speeds: Subsequently, we investigate the SER performances of the proposed OT system over the air-water interface channel with different wind speeds. In this scenario, the distance between the transceivers over the atmosphere channel is set as 100 meters and that over the underwater channel is set as 20 meters. We can observe from Fig. 14 that the system performances degrade as the sea surface wind speed increases. The reason is that the sea surface becomes rougher with higher wind speed, which leads to greater distortion degree of the propagation of light beam, thus fewer photons will reach the receiver, thereby degrading the SER performances.

4) Different MIMO orders: At last, we investigate the performances when the MIMO matrix has different dimensions while the spectrum efficiency is the same $\zeta = 8$ bit/s/Hz. More explicitly, for performance comparisons, the number of the transmit aperture is set as 8 and 16, while each user is equipped with 4 and 8 reception apertures, i.e., $p = 4$ and $p = 8$, respectively. Without loss of generality, here we choose
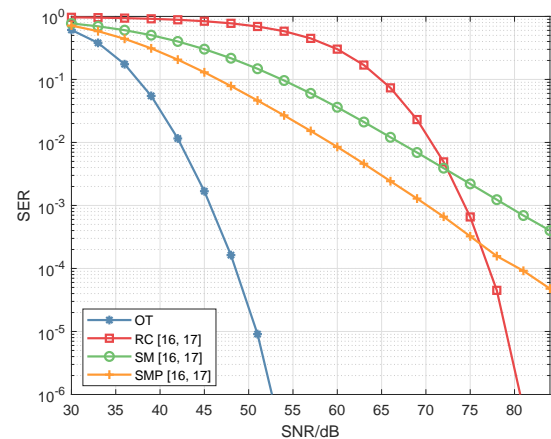

Fig. 16. Performance comparisons over the atmosphere channel, $\zeta = 8$ bit/s/Hz, $p = 8$.

Figure 15 and Fig. 16 provide the SER performance comparisons between the OT scheme and the other three benchmark schemes over the moderate ($\sigma_I^2 = 1.68$) turbulence channel with the communication distance of 500 m. The transmission spectral efficiency of each user is $\zeta = 8$ bit/s/Hz for both cases, in the case of $p = 4$, the PAM order for OT and SMP scheme is 4-PAM, for SM is 64-PAM, and for RC scheme is 256-PAM. While in the case of $p = 8$, the PAM order for OT and SMP scheme is 2-PAM, for SM is 32-PAM, and for RC scheme is 256-PAM.

From the simulation results we can see that the OT scheme still outperforms the counterpart schemes when $p > 2$, which validates the effectiveness of our proposed system. Also, it is noticeable that as the dimension of the MIMO system increases, the RC scheme would require much higher order of PAM modulations to achieve the same transmission efficiency as that of the other schemes, which leads to worse reliability performances.

Last but not the least, it is worth mentioning that in accordance with the results given in [10], we could notice that the proposed maritime VLC systems require large Γ to achieve satisfactory reliability performances of low SER, especially when delivering information over the air-water interface channel with larger path losses as demonstrated in Fig. 11. Namely, we could observe from Fig. 7, Fig. 10 and Fig. 11, which respectively investigate the SER performances over the atmosphere channel, the underwater channel and the air-water interface channel, that along with the larger path loss, the Γ required to achieve satisfactory SER also becomes larger.

V. CONCLUSION

In this paper, we propose a general orthogonal transform aided MIMO transmission scheme for maritime VLC channels to enhance the reliability performances. Practical transmission conditions are considered, including the atmosphere channel, the underwater channel as well as the air-water interface channel. With the aim to combat the attenuations induced by the complicated propagation conditions such as the absorption, turbulence, and scattering, we propose to exploit the orthogonal matrix to enlarge the Euclidean distance, and the orthogonality to suppress the interferences to enhance the reliability performances. In the proposed design, with the facility of the SVD operation, the data transmitted via MIMO channels are equivalent to be delivered in parallel. Then in order to adapt to different maritime VLC channel conditions, we propose an orthogonal transform scheme to improve the reliability performances by adjusting the orthogonal matrix $\mathbf{G}$. Furthermore, the theoretical SER expression is derived for the proposed orthogonal transform aided maritime VLC system. Numerical results demonstrate that in practical maritime scenarios, the proposed OT-aided VLC system obtains better SER performances than the counterpart systems including SMP, SM and RC aided VLC systems. Therefore, our proposed MIMO maritime VLC system can provide more reliable transmission services for user terminals.

REFERENCES

[1] N. Huang, X. Wang, and M. Chen, "Transceiver design for MIMO VLC systems with integer-forcing receivers," *IEEE J. Sel. Areas Commun.*, vol. 36, no. 1, pp. 66–77, Jan. 2018.

[2] H. Kaushal and G. Kaddoum, "Underwater optical wireless communication," *IEEE Access*, vol. 4, pp. 1518–1547, 2016.

[3] J. C. Brandenburg and J. Q. Liu, "Optical signal detection in the turbulent atmosphere using p-i-n photodiodes," *IEEE J. Sel. Areas Commun.*, vol. 27, no. 9, pp. 1564–1571, Dec. 2009.

[4] M. S. Islam, M. Younis, and A. Ahmed, "Communication through air water interface using multiple light sources," in *Proc. IEEE International Conference on Communications (ICC)*, 2018, pp. 1–6.

[5] Z. Zeng, S. Fu, H. Zhang, Y. Dong, and J. Cheng, "A survey of underwater optical wireless communications," *IEEE Commun. Surveys Tuts.*, vol. 19, no. 1, pp. 204–238, Firstquarter 2017.

[6] X. Sun, M. Kong, C. Shen, C. H. Kang, T. K. Ng, and B. S. Ooi, "On the realization of across wavy water-air-interface diffuse-line-of-sight communication based on an ultraviolet emitter," *Opt. Express*, vol. 27, no. 14, pp. 19 635–19 649, Jul. 2019.

[7] W. Liu, Z. Xu, and L. Yang, "SIMO detection schemes for underwater optical wireless communication under turbulence," *Photon. Res.*, vol. 3, no. 3, pp. 48–53, Jun. 2015.

[8] Y. Dong and J. Liu, "On BER performance of underwater wireless optical MISO links under weak turbulence," in *Proc. OCEANS, Shanghai*, Apr. 2016, pp. 1–4.

[9] M. V. Jamali, J. A. Salehi, and F. Akhoundi, "Performance studies of underwater wireless optical communication systems with spatial diversity: MIMO scheme," *IEEE Trans. Commun.*, vol. 65, no. 3, pp. 1176–1192, Mar. 2017.

[10] A. Huang, L. Tao, C. Wang, and L. Zhang, "Error performance of underwater wireless optical communications with spatial diversity under turbulence channels," *Appl. Opt.*, vol. 57, no. 26, pp. 7600–7608, Sep. 2018.

[11] D. A. Luong, T. C. Thang, and A. T. Pham, "Effect of avalanche photodiode and thermal noises on the performance of binary phase-shift keying subcarrier-intensity modulation/free-space optical systems over turbulence channels," *IET Commun.*, vol. 7, no. 8, pp. 738–744, May 2013.

[12] A. O. Aladeloba, A. J. Phillips, and M. S. Woolfson, "Improved bit error rate evaluation for optically pre-amplified free-space optical communication systems in turbulent atmosphere," *IET Optoelectron.*, vol. 6, no. 1, pp. 26–33, Feb. 2012.

[13] S. M. Navidpour, M. Uysal, and M. Kavehrad, "BER performance of free-space optical transmission with spatial diversity," *IEEE Trans. Wirel. Commun.*, vol. 6, no. 8, pp. 2813–2819, Aug. 2007.

[14] H. D. Trung, B. T. Vu, and A. T. Pham, "Performance of free-space optical MIMO systems using SC-QAM over atmospheric turbulence channels," in *Proc. IEEE International Conference on Communications (ICC)*, Jun. 2013, pp. 3846–3850.

[15] M. R. Bhatnagar and Z. Ghassemlooy, "Performance analysis of gamma–gamma fading FSO MIMO links with pointing errors," *J. Lightw. Technol.*, vol. 34, no. 9, pp. 2158–2169, May 2016.

[16] T. Fath and H. Haas, "Performance comparison of MIMO techniques for optical wireless communications in indoor environments," *IEEE Trans. Commun.*, vol. 61, no. 2, pp. 733–742, Feb. 2013.

[17] K. Cai and M. Jiang, "SM/SPPM aided multiuser precoded visible light communication systems," *IEEE Photon. J.*, vol. 8, no. 2, pp. 1–9, Apr. 2016.

[18] K. I. Gjerstad, J. J. Stamnes, B. Hamre, J. K. Lotsberg, B. Yan, and K. Stamnes, "Monte Carlo and discrete-ordinate simulations of irradiances in the coupled atmosphere-ocean system," *Appl. Opt.*, vol. 42, no. 15, pp. 2609–2622, May 2003.

[19] Y. Kaymak, R. Rojas-Cessa, J. Feng, N. Ansari, M. Zhou, and T. Zhang, "A survey on acquisition, tracking, and pointing mechanisms for mobile free-space optical communications," *IEEE Commun. Surveys Tuts.*, vol. 20, no. 2, pp. 1104–1123, 2018.

[20] S. Han, Y. Noh, R. Liang, R. Chen, Y. Cheng, and M. Gerla, "Evaluation of underwater optical-acoustic hybrid network," *China Commun.*, vol. 11, no. 5, pp. 49–59, May 2014.

[21] A. Mishra, P. S. Pati, and R. K. Giri, "Performance analysis of SIM based FSO using various modulation techniques with APD receiver over turbulent channel," in *Proc. International Conference on Wireless Communications, Signal Processing and Networking (WiSPNET)*, Mar. 2017, pp. 2730–2734.

[22] C. Gabriel, M. Khalighi, S. Bourennane, P. Leon, and V. Rigaud, "Channel modeling for underwater optical communication," in *Proc. IEEE Globecom Workshops (GC Wkshps)*, Dec. 2011, pp. 833–837.

[23] L. C. Andrews, R. L. Philips, and C. Y. Hopen, *Laser Beam Scintillation With Applications*. Bellingham, WA, USA: SPIE, 2001.

[24] Y. Fu and Y. Du, "Performance of heterodyne differential phase-shift-keying underwater wireless optical communication systems in gamma-gamma-distributed turbulence," *Appl. Opt.*, vol. 57, no. 9, pp. 2057–2063, Mar. 2018.

[25] S. Tang, Y. Dong, and X. Zhang, "Impulse response modeling for underwater wireless optical communication links," *IEEE Trans. Commun.*, vol. 62, no. 1, pp. 226–234, Jan. 2014.

[26] D. Tse and P. Viswanath, *Fundamentals of Wireless Communication*. Cambridge, UK: Cambridge University Press, 2005.

[27] G. Welti and J. Lee, "Digital transmission with coherent four - dimensional modulation," *IEEE Trans. Inf. Theory*, vol. 20, no. 4, pp. 497–502, Jul. 1974.

[28] R. Singh, T. O Farrell, and J. P. R. David, "An enhanced color shift keying modulation scheme for high-speed wireless visible light communications," *J. Lightw. Technol.*, vol. 32, no. 14, pp. 2582–2592, Jul. 2014.

[29] R. E. Caflisch, "Monte Carlo and quasi-Monte Carlo methods," *Acta Numerica*, vol. 7, p. 1–49, 1998.

[30] H. M. Oubei, J. R. Duran, B. Janjua, H. Wang, C. Tsai, Y. Chi, T. Ng, H. Kuo, J. He, M. Alouini, G. Lin, and B. S. Ooi, "4.8 gbit/s 16-QAM-OFDM transmission based on compact 450-nm laser for underwater wireless optical communication," *Opt. Express*, vol. 23, no. 18, pp. 23 302–23 309, Sep. 2015.